isvr Institute of Sound and Vibration Research

Shear Layer Refraction Corrections for Off-axis Sources in Flight Simulation: Theoretical Analysis

C.L. Morfey

ISVR Technical Report No 270

October 1997

University of Southampton

SCIENTIFIC PUBLICATIONS BY THE ISVR

Technical Reports are published to promote timely dissemination of research results by ISVR personnel. This medium permits more detailed presentation than is usually acceptable for scientific journals. Responsibility for both the content and any opinions expressed rests entirely with the author(s).

Technical Memoranda are produced to enable the early or preliminary release of information by ISVR personnel where such release is deemed to the appropriate. Information contained in these memoranda may be incomplete, or form part of a continuing programme; this should be borne in mind when using or quoting from these documents.

Contract Reports are produced to record the results of scientific work carried out for sponsors, under contract. The ISVR treats these reports as confidential to sponsors and does not make them available for general circulation. Individual sponsors may, however, authorize subsequent release of the material.

UNIVERSITY OF SOUTHAMPTON

INSTITUTE OF SOUND AND VIBRATION RESEARCH

FLUID DYNAMICS AND ACOUSTICS GROUP

Shear Layer Refraction Corrections for Off-axis Sources in Flight Simulation: Theoretical Analysis

by

C L Morfey

ISVR Technical Report No. 270

October 1997

Authorized for issue by
Professor P A Nelson
Group Chairman

Acknowledgments

Partial support for this investigation was provided by the UK Defence Evaluation Research Agency (Pyestock) through DTI CARAD. Thanks are due to Dr M J Fisher for helpful initial discussions, and to Richard Pinker for supplying background information on the Pyestock Noise Test Facility.

Contents

Abstract

A set of equations is derived for converting acoustic measurements taken in a free-jet flight simulation facility, such as the UK Noise Test Facility at Pyestock or the French CEPr at Saclay, to equivalent far-field fight conditions. The equations are based on the high-frequency geometrical acoustics approximation, whose application in the present context was justified in detail by Morfey and Tester in 1977 and by Amiet in 1978. However, the present work departs from these earlier studies by allowing the source to be positioned off the jet centreline, anywhere within the flight stream. The flight stream jet is modelled as an axisymmetric parallel shear flow, with a shear layer thickness which is small compared with the jet diameter. The model permits the microphone to be located anywhere outside the flow, arbitrarily close to the open jet. By using the results of this report, shear-layer refraction corrections can be calculated for any combination of measurement point (outside the flow) and source point (inside the flow).

I. Introduction

1. Background

The presence of installation effects, specifically the reflection or scattering of exhaust noise from the airframe structure, is now well established as an important factor which influences the community noise levels of all types of aircraft. The effects are twofold.

Firstly, the noise levels observed on the ground are often higher than would otherwise be the case. To put the point another way, the static-to-flight noise reductions predicted from flight simulation tests on an isolated exhaust system are often not realized on the installed engine.

Secondly, because installation effects are currently not well understood, their presence introduces some uncertainty into flyover noise predictions.

There is a serious difficulty in isolating installation effects from full-scale tests alone. The reason is that noise measurements at full scale are normally limited to two conditions:

- **static**, with a bare engine on a test stand, and
- **in flight**, with a fully installed engine in an aircraft.

In this situation it is impossible to decide how much of the difference in noise is due to flight effects, and how much to installation effects.

However by testing at model scale, in a flight simulation facility such as that at DERA (Pyestock), the essential four-way comparison of static and in-flight noise from both uninstalled and installed exhaust systems becomes feasible. The open-jet type of facility, in which measurements are taken outside the flight simulation stream, requires that the data be adjusted for amplitude, frequency and angle of observation in order to obtain sound pressure levels that are equivalent to flyover measurements made near the ground in the far field. In what follows, we refer to these data adjustments as "shear-layer corrections." Their calculation for off-axis sources is the subject of this report.

2. Calculation of shear-layer corrections

The standard geometrical acoustics (GA) shear layer correction procedure, for sources located on the open-jet centreline, is presented in Ref. [1]; it is valid in the limit as the sound wavelength tends to zero. Numerical calculations detailed in Refs. [1] and [2] explore the errors involved in applying the GA approximation, for cylindrical and plane shear layers respectively. In these calculations, the ratio of open-jet shear layer thickness (δ) to sound wavelength (λ) takes a range of values typical of flight test simulations. The transmitted-pressure amplitude obtained numerically differs slightly from the GA value, on account of reflections from the shear layer; the latter become more significant as the ratio δ/λ decreases. However, even in the extreme case $\delta/\lambda \rightarrow 0$, the difference between the GA and exact solutions is typically less than 0.25 dB,[†] except for sound emitted in the forward arc close to the critical angle.

[†] Calculated in Ref. [2] for $M = 0.5$ and a plane shear layer.

The shear layer corrections developed in Refs. [1] and [2] are restricted to sources on the axis of the open jet. When an installed-engine model is placed in the jet, however, the sound from a centreline engine exhaust may be scattered by surfaces relatively far from the jet axis. The question then arises of whether or not significantly different shear layer corrections are needed for these off-axis sources.

3. Scope of the investigation

In order to explore the question identified above, the standard GA correction algorithm for on-axis sources and cylindrical shear layers [1] has been extended. Sources may now be placed at arbitrary radial and azimuthal positions within the flight stream jet (the azimuthal reference being provided by the external microphone location). Chapter III sets out the theoretical basis of the generalized correction procedure, and discusses three special cases in detail:

- Measurement microphone in the geometric far field; $(r_m/a \to \infty)$
- Measurement microphone immediately outside the jet; $(r_m/a = 1)$
- Source on the jet centreline. $(r_s/a \to 0)$

Obtaining an analytical result for the general case requires a careful discussion of the ray-tube geometry, as presented in Appendix B. Note that in all cases, the general result contained in Eq. (33) of Chapter III remains valid. It relates the power spectrum of the pressure measured in the facility to the desired far-field measurement in flight. The algebraic complication which arises in the off-axis case is due entirely to the $dA_n/d\Omega_1$ term in Eq. (33), which is a measure of the ray-tube area outside the flight stream.

In a companion paper,‡ the refraction corrections described above are evaluated numerically for a range of source positions across the flight stream jet, and for a realistic range of flight Mach numbers and emission angles. The purpose is to determine whether

(a) source transverse position has too small an influence to be worth allowing for under realistic test conditions, *or*

(b) source transverse position has an appreciable influence on the interpretation of facility data. In the latter case the actual source geometry must be fed into the data correction procedure, and the results of Appendix B are needed.

‡ Oral presentation: C L Morfey, P Joseph 1997 "Shear layer corrections for off-axis sources in an open jet flight simulation facility." First CEAS–ASC Workshop (*Wind Tunnel Testing in Aeroacoustics*, 5-6 November 1997); DNW, Noordostpolder, the Netherlands.

II. List of Symbols

a	=	flight-stream nozzle radius	Fig. 3
$A(s)$	=	cross-sectional area of ray tube formed by the four rays through points B_0, B_1, B_2, B_3	App. B, Eq. (29); Figs. 5, 10
A_0, A_1, A_2	=	coefficients in $A(s)$ expression	App. B, Eqs. (30–33)
dA_m	=	ray-tube area on measurement cylinder $r = r_m$	Fig. 5
dA_n	=	ray-tube cross-sectional area at measurement position	Eq. (31)
c_1, c_0	=	sound speed inside, outside jet	
C	=	ratio of sound speeds c_1/c_0	
d_1	=	distance in transverse plane between A and B	Fig. 7; Eq. (29)
d_0	=	distance in transverse plane between B and M	Fig. 7; Eq. (29)
D_1	=	Doppler factor	Eq. (4)
E	=	$\cos\theta_0/\cos\theta_1 = (c_0/c_1)D_1$	Eqs. (9, 15)
f, f'	=	base-lengths of parallelograms $C_0C_1C_2C_3$, $B_0B_1B_2B_3$	App. B, Eq. (2)
$F(\lambda)$	=	function of azimuthal ray launch angle λ	Eq. (45)
g, g'	=	offsets of parallelograms $C_0C_1C_2C_3$, $B_0B_1B_2B_3$	App. B, Eq. (2)
G	=	$\cos\theta_0$	App. B, Eqs. (3), (34)
h, h'	=	heights of parallelograms $C_0C_1C_2C_3$, $B_0B_1B_2B_3$	App. B, Eq. (2)
H	=	ϕ_B	App. B, Eqs. (5), (36)
$\mathbf{i}_x$, $\mathbf{i}_r$, $\mathbf{i}_\phi$	=	set of orthogonal unit vectors based on coordinate directions at B	App. B, Eq. 7
$\mathbf{i}_1$, $\mathbf{i}_2$	=	orthogonal unit vectors, normal to $\mathbf{n}_0$	Figs. 11–13
k_x	=	axial wavenumber	Eq. (1)
k_1, k_0	=	acoustic wavenumbers ω_1/c_1 , ω_0/c_0	Eq. (2)
K_1, K_0	=	wavenumbers in transverse plane, for waves propagating inside and outside the flow respectively	Eqs. (5–7)
M	=	flight stream Mach number U/c_1	
$\mathbf{n}_1$, $\mathbf{n}_0$	=	unit wavenormal vectors inside, outside jet	Eqs. (14–17), (28)
P_m	=	power spectrum of acoustic pressure at measurement position M	Fig. 6; Sec. 15
P_∞	=	power spectrum of acoustic pressure under far-field flight conditions	Fig. 6; Sec. 15
Q	=	$\sin\alpha_0$	App. B, Eqs. (18), (38)
r	=	radius from jet axis	

List of Symbols

r_m	=	measurement radius outside jet	Fig. 5
r_s	=	radial position of source	Fig. 3
R_r	=	wavefront propagation distance from source, relative to fluid	Fig. 8
ΔR_r	=	correction to propagation distance	Fig. 9; Eq. (51)
R_{r0}	=	distance OM	Fig. 6; Eq. (36)
s	=	distance measured from B along ray	App. B, Eq. (45)
U	=	jet flow velocity	
v_t, v_x	=	components of **v** transverse and parallel to jet axis	Eqs. (16), (14)
v	=	ray velocity	Fig. 4
dW_1, dW_0	=	sound power in ray tube inside, outside jet	Eqs. (30–32)
x	=	axial coordinate (with source at $x = 0$)	Fig. 1
x_B	=	axial coordinate of point where ray crosses shear layer	Fig. 1; Eq. (19)
x_m	=	axial coordinate of measurement position	Eq. (28)
x_1, x_2	=	coordinates in plane normal to reference ray outside jet, with origin on the ray (at C_0)	Fig. 11
X	=	x_B/a	App. B, Eqs. (6), (41)
α_1, α_0	=	ray or wavenormal angles in plane transverse to jet axis, relative to radial direction at B (i.e. angles of incidence and transmission respectively)	Figs. 2, 3
β_1, β_0	=	$\partial\alpha_1/\partial\lambda$, $\partial\alpha_0/\partial\lambda$	App. A
δ	=	angle related to near-field geometry	Fig. 7
$\boldsymbol{\varepsilon}$, $\boldsymbol{\varepsilon}'$	=	increments in $\mathbf{n}_0$	App. B, Eq. (13)
ε_1, ε_2; ε_1', ε_2'	=	components of $\boldsymbol{\varepsilon}$ or $\boldsymbol{\varepsilon}'$ parallel to $\mathbf{i}_1$, $\mathbf{i}_2$	App. B, Eqs. (24, 25)
ξ	=	cos θ_1	App. B, Eq. (16)
θ_1, θ_0	=	wavenormal polar angles relative to jet axis, inside and outside the flow respectively	Eq. (2)
λ	=	azimuthal launch angle for ray leaving source	Fig. 3
ρ_1, ρ_0	=	fluid density inside and outside the jet	
σ	=	dimensionless radial coordinate r/a	
ϕ	=	azimuthal angle about jet axis, defined so that source is at $\phi = 0$	Fig. 1
ϕ_B	=	azimuthal position of point B where ray crosses shear layer	Fig. 3; Eq. (13)

ϕ_m	=	azimuthal position of measurement point outside shear layer	Fig. 7; Eq. (27)
ϕ_0	=	azimuthal orientation of emerging ray	Eq. (21)
ω, ω_0	=	angular frequency in a reference frame which is fixed with respect to the laboratory (or the aircraft)	Eq. (1)
ω_1	=	angular frequency in a reference frame which is fixed with respect to the flight-simulation jet flow (or the atmosphere)	
Ω	=	solid angle	
$d\Omega_1$	=	solid angle formed by a small cone of wavenormal directions leaving the source, inside the jet	Eq. (24)
$d\Omega_0$	=	solid angle formed by the corresponding rays in the far field, outside the flow	Eq. (23)

Subscripts

B	=	position B
m	=	measurement position M
r	=	radial component of vector
s	=	source position
t	=	transverse component of vector
x	=	axial component of vector
ϕ	=	azimuthal component of vector
λ, ξ	=	partial derivatives with respect to λ or ξ
1	=	value inside jet
0	=	value outside jet
∞	=	value in far field

Point labels; other abbreviations

A	=	source point	Figs. 1, 3, 9, 10
B	=	point where ray crosses jet shear layer	Figs. 1–7, 9, 10
M	=	measurement point	Figs. 6, 7, 9
N	=	corresponding measurement point in flight situation	Fig. 6
O	=	on-axis apparent origin of ray	Figs. 6, 9
GA	=	geometrical acoustics	

III. Theoretical Analysis of Refraction Corrections

1. Basis of model calculation

The following analysis is based on geometrical acoustics (GA), plus an idealized model of the flow field. Use of GA means the shear layer correction is source-independent.

Region 1 = flight simulation jet; modelled as a top-hat profile, velocity U = const.

Region 0 = exterior region, fluid at rest

x axis = downstream direction; flow field does not vary with x.

2. Angular frequencies moving with fluid

ω_0 = angular frequency relative to outer fluid (laboratory-fixed reference frame);

ω_1 = angular frequency relative to inner fluid (frame of reference moving at U).

The symbol ω without a subscript will sometimes be used in place of ω_0, where there is no risk of confusion.

3. Doppler relation

For a given wavenumber k_x,

$$\omega_0 = \omega_1 + k_x U \,. \tag{1}$$

We introduce the angles (θ_1, θ_0) defined by

$$\left.\begin{aligned} &\cos\theta_1 = k_x c_1/\omega_1 = k_x/k_1 \text{ (inside the flow)} \,, \\ &\cos\theta_0 = k_x c_0/\omega_0 = k_x/k_0 \text{ (outer region)} \,. \end{aligned}\right\} \tag{2}$$

Substituting $\omega_1 = k_x c_1/\cos\theta_1$, $\omega_0 = k_x c_0/\cos\theta_0$ in Eq. (1) gives

$$\frac{c_0}{\cos\theta_0} = \frac{c_1}{\cos\theta_1} + U \;, \text{ i.e. } \boxed{\cos\theta_0 = \frac{c_0}{c_1} D_1 \cos\theta_1} \,. \tag{3}$$

Equation (3) relates the wavenormal angles inside and outside the flow. The two frequencies are related by

$$\frac{\omega_1}{\omega_0} = D_1 = \left(1 - \frac{U}{c_0}\cos\theta_0\right) = \left(1 + \frac{U}{c_1}\cos\theta_1\right)^{-1} \tag{4}$$

The Doppler factor D_1 is the ratio of the frequency heard by an observer moving with the inner flow, and the frequency in a fixed frame.

4. Transverse wavenumbers

In the plane normal to the x axis, the wavenumbers in regions (1, 0) are denoted by K_1, K_0. They are related to k_x by

$$\left.\begin{aligned} K_1^2 + k_x^2 &= (\omega_1/c_1)^2 \ , \\ K_0^2 + k_x^2 &= (\omega_0/c_0)^2 \ . \end{aligned}\right\} \tag{5}$$

Note that the same axial wavenumber k_x applies inside and outside the jet. The (K_1, K_0) relations above can be rewritten in terms of θ_0 or θ_1, rather than k_x, by using Eqs. (2) and (4): thus

$$\left(\frac{K_1\, c_0}{\omega_0}\right)^2 = \left(\frac{c_0}{c_1}\right)^2 D_1^{\,2} - \cos^2\theta_0 \ ; \qquad \left(\frac{K_1\, c_1}{\omega_1}\right)^2 = \sin^2\theta_1 \ ; \tag{6}$$

$$\left(\frac{K_0\, c_0}{\omega_0}\right)^2 = \sin^2\theta_0 \ ; \qquad \left(\frac{K_0\, c_1}{\omega_1}\right)^2 = \left(\frac{c_1}{c_0}\right)^2 D_1^{\,-2} - \cos^2\theta_1 \ . \tag{7}$$

5. Transverse refraction

In the transverse plane, the ray emerging at B from the jet has angles of incidence and transmission (α_1, α_0) respectively, defined relative to the local normal at the interface between regions 1 and 0 (see Fig. 2).

Conservation of the transverse wavenumber parallel to the interface gives

$$K_1 \sin\alpha_1 = K_0 \sin\alpha_0 \tag{8}$$

which is a form of Snell's law. Note that the ray and wavenormal directions projected onto the transverse plane are the same, since the flow is assumed to be axial.

6. Transverse angle relation

Combining Eqs. (6)–(8), and writing $\frac{c_0}{c_1} D_1$ as E, gives

$$\left(\frac{\sin\alpha_0}{\sin\alpha_1}\right)^2 = \left(\frac{K_1}{K_0}\right)^2 = \frac{\sin^2\theta_1}{E^{-2} - \cos^2\theta_1} = \frac{E^2 - \cos^2\theta_0}{\sin^2\theta_0} \ . \tag{9}$$

Equation (9) allows rays to be traced in the transverse plane from a source at A, via the shear layer at B, to points in the exterior field.

7. Ray tracing

A ray starts from the source at A, at $(r, 0, 0)$ in cylindrical coordinates (r, ϕ, x), and crosses the jet shear layer at B. We want to find:

- The coordinates of B.
- The trajectory of the emerging ray, in terms of the ray launch angle λ in the transverse plane (see Fig. 3).

8. Azimuthal location of ray crossing

In cylindrical coordinates, Fig. 3 locates the crossing point B at

$$r_B = a \quad \text{(jet radius)}, \tag{10}$$

$$\phi_B = \lambda - \alpha_1 . \tag{11}$$

The angle of incidence α_1 is related to λ by

$$\frac{r_s}{\sin \alpha_1} = \frac{a}{\sin \lambda} ,$$

i.e. $$\sin \alpha_1 = \frac{r_s}{a} \sin \lambda . \tag{12}$$

From (11) and (12),

$$\phi_B = \lambda - \sin^{-1}\left(\frac{r_s}{a} \sin \lambda\right). \tag{13}$$

9. Axial location of ray crossing : axial ray velocity

To find x_B we need to consider the ray velocity vector **v** in the jet. Its axial component is

$$v_x = c_1 \, n_{1x} + U , \tag{14}$$

where $\mathbf{n}_1$ is the unit wavenormal vector in the flow. In terms of k_x,

$$n_{1x} = \frac{k_x}{k_1} = \frac{k_x c_1}{\omega_1} = \frac{\cos \theta_0}{E} = \cos \theta_1 , \tag{15}$$

where $E = \dfrac{k_1}{k_0} = \left(\dfrac{c_0}{c_1}\right) D_1$ was first introduced in Eq. (9).

10. Transverse ray velocity

The component of **v** in the transverse plane has magnitude

$$v_t = c_1 \, n_{1t} \tag{16}$$

where n_{1t} is the magnitude of the component of $\mathbf{n}_1$ in the transverse direction. It is related to n_{1x} and the wavenormal angles by

$$n_{1t} = \sqrt{1 - {n_{1x}}^2} = \sqrt{1 - \left(\frac{\cos \theta_0}{E}\right)^2} = \sin \theta_1 . \tag{17}$$

11. Axial distance travelled by ray in jet flow

The ratio of v_x to v_t gives the ratio of distances travelled by the ray, in a given time, parallel and perpendicular to the x axis. Thus if d_1 is the transverse distance between A and B (Fig. 3), given by

$$d_1 = a\frac{\sin\phi_B}{\sin\lambda}, \tag{18}$$

it follows that

$$\frac{x_B}{d_1} = \frac{v_x}{v_t} = \frac{c_1 n_{1x} + U}{c_1 n_{1t}}, \tag{19}$$

from Eqs. (14) and (16) above. This expression can be rewritten, using Eqs. (15) and (17), in the alternative forms

$$\frac{x_B}{d_1} = \left(\frac{\cos\theta_0}{E} + \frac{U}{c_1}\right)\Big/\sqrt{1-\left(\frac{\cos\theta_0}{E}\right)^2} = \frac{\cos\theta_1 + \frac{U}{c_1}}{\sin\theta_1}. \tag{20}$$

12. Summary of ray crossing location results

The cylindrical coordinates of the point B where the emerging ray crosses the shear layer, i.e. (x_B, ϕ_B, a), are now defined. We choose as independent variables the source radius r_s ; the ray launch angle, λ, in the transverse plane; and the wavenormal angle in the flow, θ_1, measured from the jet axis. Then:

- x_B is given by Eqs. (18) and (20) above, and
- ϕ_B is given by Eq. (13) above.

13. Ray geometry in outer region

The emerging ray outside the jet flow has a unit wavenormal vector $\mathbf{n}_0$. The direction of $\mathbf{n}_0$ can be specified in terms of azimuthal and polar angles, (ϕ_0, θ_0), as in Fig. 5. The polar angle θ_0 has already been introduced in Eq. (2), and ϕ_0 is the ray orientation in the transverse plane; it corresponds to the azimuthal coordinate of a far-field point on the ray. Thus

$$\phi_0 = \lambda - \alpha_1 + \alpha_0 \qquad \text{(see Fig. 3)}$$

$$= \lambda - \sin^{-1}\left(\frac{r_s}{a}\sin\lambda\right) + \sin^{-1}\left(\frac{K_1}{K_0}\frac{r_s}{a}\sin\lambda\right), \tag{21}$$

from Eqs. (8), (12) and (13). The polar angle θ_0 is given by

$$\cos\theta_0 = E\cos\theta_1 \quad (E = c_0 D_1/c_1)\ . \tag{22}$$

14. Ray-tube solid angles

In the far field outside the flow, the ray tube shown in Fig. 5 encloses a solid angle

$$d\Omega_0 \approx \frac{dA_m \sin^3\theta_0}{r_m^2}, \qquad (r_m/a \to \infty) \tag{23}$$

which can be expressed in terms of $d\lambda$ and $d\theta_1$ with the help of Eqs. (9), (21) and (22). The details of this calculation are deferred to Section 22.

In order to apply an energy conservation argument to relate the mean square pressures in regions (0) and (1), we shall need to calculate the ratio $dA_n/d\Omega_1$. Here dA_n is the ray tube cross-sectional area in region (0) outside the jet, which in the far field is simply related to the solid angle $d\Omega_0$ defined above; while $d\Omega_1$ is the solid angle defined by the corresponding $\mathbf{n}_1$ directions inside the jet flow. (Note that $d\Omega_1$ is *not* the ray-tube solid angle inside the jet flow, but the wavenormal solid angle.) Thus

$$d\Omega_1 = |d\lambda\, d(\cos\theta_1)| \ . \tag{24}$$

15. Facility data correction

Figure 6 shows the comparison between

(1) the ray path ABM in the flight simulation facility, and
(2) the corresponding ray path ABN in the true flight situation,

with the frame of reference in both cases chosen to make the source stationary. The power spectra of the acoustic pressure at M in the flight-simulation facility (outside the jet but not necessarily in the geometric far field), and at N in the flight situation (with the microphone in the far field), are respectively $P_m(\omega)$ and $P_\infty(\omega)$, both measured in the aircraft reference frame.

"Corresponding ray paths" means that the wavenormal $\mathbf{n}_1$ inside the flow is the same in both cases (1) and (2). Given this correspondence, the ratio $P_m(\omega)/P_\infty(\omega)$ can be predicted within the limitations of geometrical acoustics, without the need for source information.

It then follows that measured $P_m(\omega)$ values can be processed to yield $P_\infty(\omega)$.

16. Measurement practicalities

- Data are assumed to be collected at discrete points outside the open jet.
- The objective is to recover $R_r^2\, P_\infty(\omega)$ values, for selected emission angles (λ, θ_1) within the flow.
- This will involve interpolating between measurement points to get the desired (λ, θ_1) combination, and applying correction factors to the interpolated measured $P_m(\omega)$ values.

17. Relation between measurement position and source emission angles

The same cylindrical coordinates are used to locate M as were used for A and B (Figs. 1–3). Thus the (r, ϕ, x) coordinates for these points are:

(Source point A)	r_s ,	0 ,	0 ;	
(Shear layer B)	a ,	$\lambda - \alpha_1$,	x_B ,	[Eqs. (20), (18) give x_B];
(Microphone M)	r_m ,	ϕ_m ,	x_m .	

Our aim is to relate (ϕ_m, x_m) to (λ, θ_1), for given values of r_m, r_s, and a.

18. Azimuthal measurement position

From Fig. 7,

$$\phi_m = (\lambda - \alpha_1) + (\alpha_0 - \delta)\,, \tag{25}$$

where

$$\frac{a}{\sin\delta} = \frac{r_m}{\sin\alpha_0}\,. \tag{26}$$

It follows that

$$\phi_m = \lambda - \alpha_1 + \alpha_0 - \sin^{-1}\left(\frac{a}{r_m}\sin\alpha_0\right). \tag{27}$$

Note that α_1 is related to λ by Eq. (12), and α_0 to α_1 by Eq. (9). Therefore $\phi_m(\lambda, \theta_1)$ can be calculated, for any given values of r/a and r_m/a, using Eqs. (9), (12), and (27).

19. Axial measurement position

The axial displacement $x_m - x_B$ follows from a calculation similar to that used earlier to find x_B (see Sections 9 to 11); but since this segment of the ray path lies outside the jet, there is no complication arising from flow convection. Thus

$$\frac{x_m - x_B}{d_0} = \frac{n_{0x}}{n_{0t}} = \frac{\cos\theta_0}{\sin\theta_0} = \frac{E\cos\theta_1}{\sqrt{1 - E^2\cos^2\theta_1}}\,. \tag{28}$$

The distance d_0 is the projection of BM on the transverse plane (see Fig. 7); using Eqs. (25) to (27) gives

$$\begin{aligned} d_0 &= r_m \frac{\sin(\alpha_0 - \delta)}{\sin\alpha_0} \\ &= r_m \cdot \frac{1}{\sin\alpha_0}\sin\left\{\alpha_0 - \sin^{-1}\frac{a}{r_m}\sin\alpha_0\right\}. \end{aligned} \tag{29}$$

As was noted in Section 18, α_0 can be found from (λ, θ_1). Therefore Eqs. (28) and (29) allow $(x_m - x_B)/a$ to be calculated, as a function of (λ, θ_1) and the parameters $(r_s/a, r_m/a)$.

20. Amplitude correction

The analysis of Sections 17–19 allows the ray position (ϕ_m, x_m) to be identified, on the near-field cylindrical surface $r = r_m$, for any combination of source emission angles (λ, θ_1) in the jet flow. The next step is to convert the measured $P_m(\omega)$ value to an equivalent $R_r^2\, P_\infty(\omega)$ value in the true flight situation.

The approach adopted is that used in Ref. [1]. Based on the GA approximation, the acoustic energy flow along a ray tube – such as that in Fig. 5 – is conserved. If $dW_1(\omega)$ denotes the power travelling along section AB of the ray tube, per unit angular frequency in a reference

frame attached to the facility (or aircraft), and $dW_0(\omega)$ is the power in the same ray tube after it emerges from the jet, then energy conservation means that

$$dW_1(\omega) = dW_0(\omega) \ . \tag{30}$$

(1) Outside the flow, $dW_0(\omega)$ is related to the measured power spectrum of acoustic pressure $P_m(\omega)$ as follows:

$$dW_0(\omega) = \frac{dA_n}{\rho_0 \, c_0} P_m(\omega) \tag{31}$$

Here dA_n is the ray-tube cross-sectional area (measured normal to the ray direction), at the measurement location M outside the jet (see Figs. 6 and 7). It is not the same as dA_m (measured on the cylindrical surface $r = r_m$; see Fig. 5).

(2) Inside the flow, $dW_1(\omega)$ is related to the far-field quantity $R_r^2 \ P_\infty(\omega)$ that would ideally be measured in the true flight situation. The distance R_r is the distance travelled by an acoustic wavefront relative to the fluid, as indicated in Fig. 8. The relationship is

$$dW_1(\omega) = \frac{d\Omega_1}{\rho_1 \, c_1 \, D_1^{\,2}} R_r^2 \ P_\infty(\omega) \ , \tag{32}$$

and follows from Eq. (15) of Ref. [1].

Equating expressions (31) and (32) gives

$$\boxed{R_r^2 \ P_\infty(\omega) = \frac{\rho_1 \, c_1 \, D_1^{\,2}}{\rho_0 c_0} \ . \ \frac{dA_n}{d\Omega_1} \ . \ P_m(\omega)} \tag{33}$$

This is a key result, as it provides a conversion from the near-field measurement $P_m(\omega)$ made in the facility outside the shear layer, to the desired far-field measurement that would be made in the true flight situation without the shear layer. The frame of reference in both cases is attached to the source (aircraft).

21. Calculation of $dA_n/d\Omega_1$ factor

The solid angle $d\Omega_1$ is related to the incremental source emission angles, $d\lambda$ and $d\theta_1$, by Eq. (24). However, the cross-sectional area dA_n of the emerging ray tube in the geometric near field is a complicated function of several variables:

$$dA_n = a^2 \, d\lambda \, d\theta_1 \ . \ f(\lambda, \ \theta_1, \ U_1/c_1, \ c_0/c_1, \ r_s/a, \ r_m/a) \ . \tag{34}$$

There are two special cases where $dA_n/d\Omega_1$ is relatively straightforward to calculate, and which can be used to test any subsequent approximations: they are

(1) Measurement position immediately outside the shear layer, i.e. at point B in Figs. 1–7;

(2) Source position on the jet centreline.

The exact calculations for these two cases are presented in Sections 24 and 25. In Section 22 below we present an approximation which is asymptotically valid in the far field, and which is relatively simple to derive; the general exact result, which can be obtained analytically but is considerably more complicated, is developed in Appendix B.

22. Approximation to $dA_n/d\Omega_1$ factor

For distances r_m from the jet axis which are not too small (say $r_m/a > 10$), it may be sufficiently accurate to estimate dA_n from the far-field expression

$$dA_n \approx R_{r0}^2 \, d\Omega_0 \, . \tag{35}$$

Here $d\Omega_0$ is the ray-tube solid angle in the outer region [region (0)]. Further information on ray geometry in this region, in the far-field limit, is provided in Fig. 5 and Section 13. The distance R_{r0} is shown as OM in Fig. 6; it is based on projecting the far-field refracted ray back to the jet axis, and is given by

$$R_{r0} = \frac{r_m}{\sin \theta_0} \, . \tag{36}$$

From Eqs. (23), (35) and (36), we get the approximate relation

$$\frac{dA_n}{r_m^2} \approx \sin \theta_0 \left(\frac{dA_m}{r_m^2} \right)_{r_m \to \infty} \, . \tag{37}$$

The $\sin \theta_0$ factor in this result is expected, since dA_m has its normal at angle θ_0 to the ray direction.

The last factor on the right of Eq. (37) is evaluated in Appendix A. Combining Eq. (9) from Appendix A with Eq. (37) above gives

$$\boxed{\frac{dA_n}{r_m^2} \approx \left(1 - \beta_1 + \beta_0\right) \frac{c_1}{c_0} \frac{E^2 \sin \theta_1}{1 - E^2 \cos^2 \theta_1} \, d\lambda \, d\theta_1 \, .} \tag{38}$$

As a check on this result, we note that for on-axis sources (i.e. $\beta_1 = \beta_0 = 0$) it reproduces the exact far-field expression

$$\left(\frac{dA_n}{R_{r0}^2} \right)_{\text{far field}} = d\Omega_0 = d\lambda \, . \sin \theta_0 \, d\theta_0 \, . \tag{39}$$

The equivalence of Eqs. (38) and (39) in this situation can be demonstrated by first using Eq. (36) to replace R_{r0}, and then using Eq. (3) above with Eq. (6) from Appendix A to replace θ_0 by θ_1.

Finally, when Eqs. (24) and (38) are used to substitute for $d\Omega_1$ and dA_n in Eq. (33), we obtain the following *approximate* equation for correcting measured power spectra to their equivalent far-field flight values:

$$R_r^2\, P_\infty(\omega) = \frac{\rho_1}{\rho_0} D_1^4 \frac{r_m^2\, P_m(\omega)}{1 - \left(\frac{c_0}{c_1} D_1 \cos\theta_1\right)^2} \left(1 - \beta_1 + \beta_0\right) . \tag{40}$$

As mentioned above, the exact version of Eq. (40) is given in Appendix B. An interpretation of the various factors in Eq. (40) is presented in the following sections.

23. Interpretation of the flight-facility amplitude correction equation

- Equation (40), or its generalized version Eq. (33), converts power spectra of sound pressure measured outside the jet, on a cylinder of radius r_m concentric with the jet axis, to equivalent far-field flight values.
- The measurement location on the cylinder $r = r_m$ is chosen to correspond with the desired source emission angles (λ, θ_1). For this purpose, microphone coordinates (ϕ_m, x_m) are chosen as described in Sections 17–19.
- The polar emission angle θ_1 is the wavenormal polar angle within the jet flow, referred to a polar axis pointing in the flight stream direction. It also corresponds to the flyover polar angle based on the aircraft position at the emission time.
- The far-field distance R_r is the distance travelled by the wavefronts in the true flight situation. In aircraft coordinates, the atmosphere is moving and R_r is the distance travelled relative to the fluid. Note that for an aircraft flying past a fixed observer in a still atmosphere, R_r is the source-observer distance in the far field, measured at the emission time.
- The final factor on the right of Eq. (40) accounts for off-axis source locations. It is an approximation, valid when r_m/a is greater than 3 or so, which can be checked against the exact special-case results presented below.
- The next-to-last factor in Eq. (40) represents $R_{r0}^2\, P_m(\omega)$.
- The factor $(\rho_1/\rho_0)D_1^4$ is what was called the "facility correction factor" in Ref. [1]. It represents the amplitude correction factor, for on-axis sources and a far-field observer, required to correct for refraction through the shear layer after scaling for distance by $(R_{r0}/R_r)^2$.
- All frequencies in Eq. (40), or its generalized version Eq. (33), are measured relative to the source (aircraft). Using a ground-based microphone is equivalent to measuring the frequency relative to the flow, and yields Doppler shifted frequencies $D_1\omega = \omega_1$. Thus if $P_g(\omega_1)$ is the power spectrum measured by a ground-based observer at the same emission distance R_r, the two power spectra are related by

$$\omega_1\, P_g(\omega_1) = \omega\, P_\infty(\omega) . \tag{41}$$

Equation (41) implies that proportional-bandwidth levels (measured in 1/3-octave bands, for example) are the same for both observers.

- One may wish to convert proportional-band facility measurements at frequency ω into equivalent far-field flyover data at ω_1, as measured by a stationary observer on the ground. It follows from Eqs. (33) and (41) that

$$R_r^2\ \omega_1\ P_g(\omega_1) = \frac{\rho_1\ c_1\ D_1^2}{\rho_0\ c_0}\ .\ \frac{dA_n}{d\Omega_1}\quad \omega P_m(\omega) \tag{42}$$

The angular frequencies which appear in Eq. (42) may conveniently be replaced by ordinary frequencies in Hz.

24. Near-field test of ray-tube area approximation: (i) Measurements immediately outside jet shear layer

It is straightforward to calculate dA_n exactly for points immediately outside the shear layer ($r_m = a$), noting that dA_n is then related to dA_m by $dA_n = dA_m\ n_{0r} = dA_m \sin\theta_0 \cos\alpha_0$. The area A_m on the cylinder $r = r_m$ is given, for the special case $r_m = a$, by

$$dA_m = a\ |d\phi_B\ dx_B| \tag{43}$$

where

$$d\phi_B = \left(\frac{\partial\phi_B}{\partial\lambda}\right)_{\theta_1} d\lambda\ ,\quad dx_B = \left(\frac{\partial x_B}{\partial\theta_1}\right)_{\lambda} d\theta_1 \tag{44}$$

and ϕ_B, x_B are given by Eqs. (13), (20) and (18). It follows that

$$d\phi_B = \left\{1 - \frac{\frac{r_s}{a}\cos\lambda}{\sqrt{1-\left(\frac{r_s}{a}\sin\lambda\right)^2}}\right\} d\lambda = F(\lambda)\,d\lambda\ \text{(say)}\ ; \tag{45}$$

$$dx_B = -a\,\frac{\sin\phi_B}{\sin\lambda}\,\frac{1+\frac{U}{c_1}\cos\theta_1}{\sin^2\theta_1}\,d\theta_1\ . \tag{46}$$

Finally, substituting Eqs. (45, 46) in Eq. (43) gives

$$dA_m = a^2\,F(\lambda)\,\frac{\sin\phi_B}{\sin\lambda}\,\frac{d\lambda\,d\theta_1}{D_1\sin^2\theta_1}\ . \tag{47}$$

The ray-tube area dA_n ($= dA_m \sin\theta_0 \cos\alpha_0$) follows directly. We can now combine Eq. 47) with the ϕ_B equation (13) and the α_0 equation

$$\sin^2\alpha_0 = \frac{\sin^2\theta_1}{E^{-2}-\cos^2\theta_1}\left(\frac{r_s}{a}\right)^2\sin^2\lambda \tag{48}$$

—which follows from Eqs. (8), (9) and (12)—to obtain the exact ray-tube area at point B immediately outside the shear layer. Comparison with Eq. (38) provides the first check on the

approximate ray-tube area. Thus for comparison purposes, we rewrite the exact result at $r_m = a$ as

$$\frac{dA_n}{r_m^2} = F(\lambda)\frac{\sin\phi_B}{\sin\lambda}\cos\alpha_0 \cdot \frac{c_0}{c_1}\frac{\sin\theta_0}{\cos\theta_0}\frac{\cos\theta_1}{\sin^2\theta_1}\,d\lambda\,d\theta_1 \tag{49}$$

The first 3 factors on the right of Eq. (49) are equal to 1 for on-axis sources; this fact is used below in Section 25, to provide a cross-check on Eq. (49).

25. Near-field test of ray-tube area approximation: (ii) Source on jet axis

A second exact expression for dA_n can be found by limiting the source position to the jet axis; in this case there is no restriction on the measurement distance from the axis, beyond $r_m > a$. The ray-tube area is given by

$$dA_n = R_{r0}\,(R_{r0} + \Delta R_r)\sin\theta_0\,|d\theta_0\,d\lambda|\ , \tag{50}$$

where ΔR_r is defined in Fig. 9. From Eq. (29) of Ref. [1],

$$\Delta R_r = \frac{a}{\sin\theta_0}\left[\left(\frac{\tan\theta_0}{\tan\theta_1}\right)^3\left(\frac{c_0}{c_1}\right)^2 - 1\right]. \tag{51}$$

Equation (6) of Appendix A gives

$$\sin\theta_0\,d\theta_0 = \frac{c_1}{c_0}\frac{\cos^2\theta_0}{\cos^2\theta_1}\sin\theta_1\,d\theta_1\ , \tag{52}$$

and R_{r0} is defined by Eq. (36). Combining these results gives

$$\frac{dA_n}{r_m^2} = \left\{1 + \frac{a}{r_m}\left[\left(\frac{\tan\theta_0}{\tan\theta_1}\right)^3\left(\frac{c_0}{c_1}\right)^2 - 1\right]\right\}\frac{c_1}{c_0}\frac{\cos^2\theta_0}{\sin^2\theta_0}\frac{\sin\theta_1}{\cos^2\theta_1}\,d\lambda\,d\theta_1 \tag{53}$$

which gives dA_n exactly for on-axis sources. The corresponding approximate expression, obtained from Eq. (38) by putting the source on-axis, is

$$\frac{dA_n}{r_m^2} \approx \frac{c_1}{c_0}\frac{\cos^2\theta_0}{\sin^2\theta_0}\frac{\sin\theta_1}{\cos^2\theta_1}\,d\lambda\,d\theta_1\ . \tag{54}$$

For on-axis sources, the only difference between the exact expression (53) and the approximation of Eq. (54) above is the factor in curly brackets. This observation suggests that the more general approximate expression in Eq. (38) could be improved simply by inserting the curly-bracketed factor from Eq. (53).

In the special case $r_m = a$ considered in the previous section, this bracketed factor takes the value

$$\{\ \ldots\ \} = \left(\frac{\tan\theta_0}{\tan\theta_1}\right)^3\left(\frac{c_0}{c_1}\right)^2. \tag{55}$$

Therefore for a combination of (i) measurement position immediately outside the shear layer and (ii) on-axis sources,

$$\frac{dA_n}{r_m^2} = \frac{c_0}{c_1} \frac{\sin \theta_0}{\cos \theta_0} \frac{\cos \theta_1}{\sin^2 \theta_1} d\lambda \, d\theta_1 \, . \tag{56}$$

This special case of Eq. (53) agrees exactly with the on-axis version of Eq. (49), which was derived for any source position and $r_m = a$.

IV. Summary and Conclusions

1. A simplified model of the open-jet type of flight simulation facility has been used to study the refraction corrections needed for sources located off the flight-stream axis.

2. The mean flow model consists of a uniform parallel jet, separated from the outer stationary fluid by a thin shear layer. The density and sound speed in the jet are allowed to be different from those in the ambient fluid.

3. The acoustic model consists of a point source of arbitrary directivity, located at any position within the jet, and radiating to any position in the outer fluid (i.e. including the geometric near field).

4. The calculation is based on the geometrical acoustics (GA) approximation, and so contains no explicit frequency dependence in the predicted refraction corrections. The GA approximation is valid at high frequencies, and strictly requires the acoustic wavelength to be much less than the shear layer thickness at the edge of the flight stream. A detailed comparison is presented in Ref. [1] between the GA method and a wave-theory numerical calculation for on-axis sources, using realistic ratios of shear-layer thickness to wavelength; it shows close agreement between the two transmitted pressure levels, even for single-frequency sources. For finite-bandwidth data (e.g. 1/3-octave) the agreement will be closer still.

5. The GA calculation uses ray tracing to identify what microphone positions outside the jet correspond to specified source emission angles inside the flow. Exact analytical expressions are presented for this purpose in Equations (27-29) and Eq. (20) of Chapter III.

6. Amplitude corrections are then applied along each ray path, to convert facility measurements taken at a finite distance from the jet axis to equivalent far-field flight conditions. The generalized correction procedure is summarized in Equation (33) and Section 23 of Chapter III.

7. The influence of off-axis source positions, on the far-field in-flight noise levels which are inferred from facility data, arises in two distinct ways:

   (a) The required microphone position outside the jet, for a fixed source emission direction and for measurements at a given distance from the axis, will differ according to the transverse source location.

   (b) There is a ray-tube area factor in Eq. (33), whose value depends on source radial position within the jet.

8. The area factor mentioned above is calculated explicitly in Appendix B. The general result, given in Eq. (44) of Appendix B, reduces in the appropriate limiting cases to results given in Chapter III.

9. In order to assess the magnitude of the effects due to off-axis source location, a numerical study has been carried out over a range of Mach numbers and geometrical parameter values. The results of this study will be presented in a companion paper.

References

[1] MORFEY C.L. and TESTER B.J. 1977 Noise measurements in a free jet flight simulation facility: Shear layer refraction and facility-to-flight corrections. *Journal of Sound and Vibration* **54**(1), 83-106.

[2] AMIET R. K. 1978 Refraction of sound by a shear layer. *Journal of Sound and Vibration* **58**(4), 467-482.

APPENDIX A : Ray-tube area calculation in the far field

The area dA_m, defined in Fig. 5, has a far-field asymptotic value

$$dA_m \approx r_m \, |d\phi_0 \, dx_0| \tag{1}$$

where

$$d\phi_0 = \left.\frac{\partial \phi_0}{\partial \lambda}\right|_{\theta_1} d\lambda \,, \tag{2}$$

$$dx_0 = \left.\frac{\partial x_0}{\partial \theta_1}\right|_{\lambda} d\theta_1 \,; \tag{3}$$

the far-field azimuthal angle ϕ_0 is given by Eq. (21) of Chapter III for finite r_s/a, and the far-field axial ray displacement x_0 is

$$x_0 = r_m \cot \theta_0 \,. \tag{4}$$

Thus

$$\left.\frac{\partial x_0}{\partial \theta_1}\right|_{\lambda} = -\, r_m \csc^2 \theta_0 \frac{d\theta_0}{d\theta_1}, \tag{5}$$

where $d\theta_0/d\theta_1$ follows from the differential version of Eq. (3), Chapter III:

$$c_0 \frac{\sin \theta_0}{\cos^2 \theta_0} d\theta_0 = c_1 \frac{\sin \theta_1}{\cos^2 \theta_1} d\theta_1 \,. \tag{6}$$

Combining the last two equations gives

$$\left.\frac{\partial x_0}{\partial \theta_1}\right|_{\lambda} = -\, r_m \frac{c_1}{c_0} \frac{\cos^2 \theta_0}{\sin^3 \theta_0} \frac{\sin \theta_1}{\cos^2 \theta_1} \,. \tag{7}$$

Also, since K_1/K_0 depends on θ_1 but not on λ [as Eq. (9) demonstrates], differentiating Eq. (21) gives

$$\begin{aligned} \left.\frac{\partial \phi_0}{\partial \lambda}\right|_{\theta_1} &= 1 - \left[1 - \left(\frac{r_s}{a}\right)^2 \sin^2 \lambda\right]^{-1/2} \frac{r_s}{a} \cos \lambda + \left[1 - \left(\frac{K_1}{K_0}\right)^2 \left(\frac{r_s}{a}\right)^2 \sin^2 \lambda\right]^{-1/2} \frac{K_1}{K_0} \frac{r_s}{a} \cos \lambda \\ &= 1 - \beta_1 + \beta_0, \end{aligned} \tag{8}$$

where $\beta_1 = \partial \alpha_1 / \partial \lambda$ and $\beta_0 = \partial \alpha_0 / \partial \lambda$.

It follows from these results that in the far field ($r_m/a \to \infty$),

$$\begin{aligned} dA_m &\approx r_m^2 \frac{c_1}{c_0} \frac{\cos^2 \theta_0}{\sin^3 \theta_0} \frac{\sin \theta_1}{\cos^2 \theta_1} (1 - \beta_1 + \beta_0) . |d\lambda \, d\theta_1| \\ &\approx \frac{r_m^2}{\sin \theta_0} (1 - \beta_1 + \beta_0) \frac{c_1}{c_0} \frac{E^2 \sin \theta_1}{1 - E^2 \cos^2 \theta_1} |d\lambda \, d\theta_1| \,. \end{aligned} \tag{9}$$

In Eq. (9), the relation $\cos \theta_0 = E \cos \theta_1$ from Eq. (15) has been used to replace θ_0 by θ_1.

APPENDIX B : Ray-tube area calculation in the general case

1. The ray tube shown in Fig. 10 is defined by the following four emission directions from the source at A:

Ray 0 (the reference ray)	θ_1 ,	λ ;
Ray 1	$\theta_1 + d\theta_1$,	λ ;
Ray 2	θ_1 ,	$\lambda + d\lambda$;
Ray 3	$\theta_1 + d\theta_1$,	$\lambda + d\lambda$. (1)

The intersection of the ray tube with the cylinder $r = a$ defines a parallelogram $B_0 B_1 B_2 B_3$.

2. Figure 11 shows a cross-section of the emerging ray tube in the vicinity of B just outside the jet, normal to the unit vector $\mathbf{n}_0$ (the emerging ray direction). The cross-section $C_0 C_1 C_2 C_3$ is the projection of $B_0 B_1 B_2 B_3$ onto the plane normal to $\mathbf{n}_0$. Our aim in this Appendix is to calculate the cross-sectional area $A(s)$ of the spreading ray tube, as a function of distance s measured along the ray from B. Note that $A(0)$ is equal to fh, where f is measured in the $\mathbf{i}_1$ direction and h in the $\mathbf{i}_2$ direction; see Fig. 11. The unit vector $\mathbf{i}_1$ is defined to be perpendicular to $\mathbf{n}_0$ and coplanar with $(\mathbf{n}_0, \mathbf{i}_x)$, where $\mathbf{i}_x$ is the unit vector in the x direction. The unit vectors $(\mathbf{i}_1, \mathbf{i}_2, \mathbf{n}_0)$ form a right-handed orthogonal set. They are further illustrated in Figs. 12 and 13.

3. The dimensions f, g, h of the parallelogram $C_0 C_1 C_2 C_3$ in Fig. 11 are related to the corresponding dimensions f', g', h' of the parallelogram $B_0 B_1 B_2 B_3$ by

$$f = f' \sin\theta_0 \ , \ g = g' \sin\theta_0 \ , \ h = h' \cos\alpha_0 \ . \tag{2}$$

4. The ray direction outside the jet is given by (θ_0, ϕ_0). These angles are determined by the angles (θ_1, λ) at which the ray is emitted inside the jet. Note that ϕ_0 is not the *coordinate* of a point on the ray, but the ray *orientation* relative to $\phi = 0$. The required relations are –

$$\cos\theta_0 = G(\xi, \frac{u}{c_1}, \frac{c_1}{c_0}) \ , \quad (\xi = \cos\theta_1) \ ; \tag{3}$$

$$\phi_0 = \lambda - \sin^{-1}\left(\frac{r_s}{a}\sin\lambda\right) + \alpha_0 \ . \tag{4}$$

For details, see Eqs. (21, 22), (6, 7) and (4) of Chapter III.

5. It is convenient to locate points (B_0, B_1, B_2, B_3) on $r = a$ by means of their cylindrical coordinates (x_B, ϕ_B). From Eq. (13) of Chapter III, we obtain

$$\phi_B = H(\lambda, \frac{r_s}{a}) \ ; \tag{5}$$

also

$$\frac{x_B}{a} = X(\xi, \lambda, \frac{u}{c_1}, \frac{r_s}{a}) \ , \tag{6}$$

as follows from Chapter III, Eqs. (20), (18).

6. The emerging ray direction $\mathbf{n}_0(\xi, \lambda)$ is conveniently specified in cylindrical components, based on the (ϕ, r) coordinate directions at point B:

$$(\mathbf{n}_0)_x = \cos\theta_0\,,\ (\mathbf{n}_0)_\phi = \sin\theta_0 \sin\alpha_0\,,\ (\mathbf{n}_0)_r = \sin\theta_0 \cos\alpha_0\,. \tag{7}$$

Here angle α_0 is defined in Figs. 3 and 12. The set of unit vectors $(\mathbf{i}_x, \mathbf{i}_\phi, \mathbf{i}_r)$ is defined to correspond with the local coordinate directions (x, ϕ, r).

7. In what follows, we shall need to convert between local (x, ϕ, r) components, based on the $(\mathbf{i}_x, \mathbf{i}_\phi, \mathbf{i}_r)$ unit vectors defined above, and components based on the alternative $(\mathbf{i}_1, \mathbf{i}_2, \mathbf{n}_0)$ system. We therefore begin by expressing $\mathbf{i}_1$ and $\mathbf{i}_2$ in terms of the former system. The unit vector $\mathbf{i}_2$ is given by $(\mathbf{n}_0 \times \mathbf{i}_x) / |\mathbf{n}_0 \times \mathbf{i}_x|$, where

$$(\mathbf{n}_0 \times \mathbf{i}_x) = (\mathbf{i}_x \cos\theta_0 + \mathbf{i}_\phi \sin\theta_0 \sin\alpha_0 + \mathbf{i}_r \sin\theta_0 \cos\alpha_0) \times \mathbf{i}_x$$

$$= \mathbf{i}_\phi \sin\theta_0 \cos\alpha_0 - \mathbf{i}_r \sin\theta_0 \sin\alpha_0\,. \tag{8}$$

It follows that

$$|\mathbf{n}_0 \times \mathbf{i}_x| = \sin\theta_0. \tag{9}$$

Thus

$$\mathbf{i}_2 = \mathbf{i}_\phi \cos\alpha_0 - \mathbf{i}_r \sin\alpha_0\,. \tag{10}$$

8. The unit vector $\mathbf{i}_1$ is given by

$$\mathbf{i}_1 = \mathbf{i}_2 \times \mathbf{n}_0\,. \tag{11}$$

Thus Eqs. (7) and (11) give

$$\mathbf{i}_1 = (\mathbf{i}_\phi \cos\alpha_0 - \mathbf{i}_r \sin\alpha_0) \times (\mathbf{i}_x \cos\theta_0 + \mathbf{i}_\phi \sin\theta_0 \sin\alpha_0 + \mathbf{i}_r \sin\theta_0 \cos\alpha_0)$$

$$= \mathbf{i}_x (\sin\theta_0 \cos^2\alpha_0 + \sin\theta_0 \sin^2\alpha_0) + \mathbf{i}_\phi (-\cos\theta_0 \sin\alpha_0) + \mathbf{i}_r (-\cos\theta_0 \cos\alpha_0)$$

$$= \mathbf{i}_x \sin\theta_0 - \mathbf{i}_\phi \cos\theta_0 \sin\alpha_0 - \mathbf{i}_r \cos\theta_0 \cos\alpha_0\,. \tag{12}$$

It is easy to verify that $\mathbf{i}_1 \cdot \mathbf{i}_2 = 0$, as expected.

9. Calculating the ray-tube area outside the jet (beyond point B) requires a knowledge of the separate directions of the 4 neighbouring rays. We therefore define the unit-vector increments $(\boldsymbol{\varepsilon}, \boldsymbol{\varepsilon}')$ as follows:

$$\mathbf{n}_0 \text{ (ray 1)} - \mathbf{n}_0 \text{ (ray 0)} = \boldsymbol{\varepsilon}\,, \quad \mathbf{n}_0 \text{ (ray 2)} - \mathbf{n}_0 \text{ (ray 0)} = \boldsymbol{\varepsilon}'\,. \tag{13}$$

These increments are special cases of the general relation

$$d\mathbf{n}_0 = d\{(\mathbf{i}_x \cos\theta_0 + \mathbf{i}_\phi \sin\theta_0 \sin\alpha_0 + \mathbf{i}_r \sin\theta_0 \cos\alpha_0)\}$$

$$= \mathbf{i}_x\, d(\cos\theta_0) + \mathbf{i}_\phi\, [d(\sin\theta_0 \sin\alpha_0) + \sin\theta_0 \cos\alpha_0\, d\phi_B]$$

$$+ \mathbf{i}_r\, [d(\sin\theta_0 \cos\alpha_0) - \sin\theta_0 \sin\alpha_0\, d\phi_B]\,. \tag{14}$$

The last step above involves the relations

$$d\mathbf{i}_x = 0\,, \quad d\mathbf{i}_\phi = (-\,d\phi_B)\,\mathbf{i}_r\,, \quad d\mathbf{i}_r = (d\phi_B)\,\mathbf{i}_\phi \tag{15}$$

for the basis vector increments due to a shift in the ray crossing point B: the 4 rays cross $r = a$ at four different positions (B_0, B_1, B_2, B_3), and the differences in ϕ_B produce differences in $\mathbf{i}_\phi$ and $\mathbf{i}_r$.

10. From Eq. (3) above, with cos θ_1 written as ξ,

$$d(\cos\theta_0) = \frac{\partial G}{\partial \xi}\,d\xi\,; \quad d(\sin\theta_0) = -\cot\theta_0\, d(\cos\theta_0)\,. \tag{16}$$

Also, to evaluate Eq. (14) we need an expression for $d\alpha_0$. Equation (21) of Chapter III gives

$$\sin\alpha_0 = \frac{K_1}{K_0}\frac{r_s}{a}\sin\lambda = Q\left(\lambda\,,\ \xi\,,\ \frac{U}{c_1}\,,\ \frac{c_1}{c_0}\,,\ \frac{r_s}{a}\right)\,. \tag{17}$$

Therefore

$$d(\sin\alpha_0) = \frac{\partial Q}{\partial \xi}d\xi + \frac{\partial Q}{\partial \lambda}d\lambda\,; \quad d(\cos\alpha_0) = -\tan\alpha_0\, d(\sin\alpha_0)\,. \tag{18}$$

11. The next step is to express $d\mathbf{n}_0$ and hence (ε, ε') in terms of ($d\xi$, $d\lambda$), using Eqs. (5) and (14) to (18) above:

$$d\mathbf{n}_0(d\xi, d\lambda) = \mathbf{i}_x\, G_\xi\, d\xi$$

$$+\,\mathbf{i}_\phi\,[\sin\theta_0\,(Q_\xi\,d\xi + Q_\lambda\,d\lambda) + \sin\theta_0\cos\alpha_0\,H_\lambda\,d\lambda - \sin\alpha_0\cot\theta_0\,G_\xi\,d\xi\,]$$

$$+\,\mathbf{i}_r\,[-\sin\theta_0\tan\alpha_0\,(Q_\xi\,d\xi + Q_\lambda\,d\lambda) - \sin\theta_0\sin\alpha_0\,H_\lambda\,d\lambda - \cos\alpha_0\cot\theta_0\,G_\xi\,d\xi]; \tag{19}$$

$$\varepsilon = d\mathbf{n}_0(d\xi, 0)\,, \quad \varepsilon' = d\mathbf{n}_0(0, d\lambda)\,. \tag{20}$$

12. To calculate $A(s)$, we shall need the components of ε, ε' in the $\mathbf{i}_1$ and $\mathbf{i}_2$ directions. The scalar products of $d\mathbf{n}_0$ with ($\mathbf{n}_0$, $\mathbf{i}_1$, $\mathbf{i}_2$) are:

$$\mathbf{n}_0\cdot d\mathbf{n}_0 = \{G_\xi\cos\theta_0 + [Q_\xi\sin\theta_0 - G_\xi\sin\alpha_0\cot\theta_0]\sin\theta_0\sin\alpha_0$$
$$+\,[-\,Q_\xi\tan\alpha_0\sin\theta_0 - G_\xi\cos\alpha_0\cot\theta_0]\sin\theta_0\cos\alpha_0\}\,d\xi$$
$$+\,\{[Q_\lambda\sin\theta_0 + H_\lambda\sin\theta_0\cos\alpha_0]\sin\theta_0\sin\alpha_0$$
$$+\,[-\,Q_\lambda\tan\alpha_0\sin\theta_0 - H_\lambda\sin\alpha_0\sin\theta_0]\sin\theta_0\cos\alpha_0\}\,d\lambda$$
$$= 0\,, \text{ as expected}\,; \tag{21}$$

$$\mathbf{i}_1\cdot d\mathbf{n}_0 = \{G_\xi\sin\theta_0 + [-\,Q_\xi\sin\theta_0 + G_\xi\sin\alpha_0\cot\theta_0]\cos\theta_0\sin\alpha_0$$
$$+\,[Q_\xi\tan\alpha_0\sin\theta_0 + G_\xi\cos\alpha_0\cot\theta_0]\cos\theta_0\cos\alpha_0\}\,d\xi$$
$$+\,\{-[Q_\lambda\sin\theta_0 + H_\lambda\sin\theta_0\cos\alpha_0]\cos\theta_0\sin\alpha_0$$
$$+\,[Q_\lambda\tan\alpha_0\sin\theta_0 + H_\lambda\sin\alpha_0\sin\theta_0]\cos\theta_0\cos\alpha_0\}\,d\lambda$$

$$= \frac{1}{\sin\theta_0} G_\xi \, d\xi \, ; \tag{22}$$

$$\mathbf{i}_2 \cdot d\mathbf{n}_0 = \{[Q_\xi \sin\theta_0 - G_\xi \cot\theta_0 \sin\alpha_0] \cos\alpha_0 + [Q_\xi \sin\theta_0 \tan\alpha_0 + G_\xi \cot\theta_0 \cos\alpha_0] \sin\alpha_0\} \, d\xi$$

$$+ \{ [Q_\lambda \sin\theta_0 + H_\lambda \sin\theta_0 \cos\alpha_0] \cos\alpha_0 + [Q_\lambda \sin\theta_0 \tan\alpha_0 + H_\lambda \sin\theta_0 \sin\alpha_0] \sin\alpha_0\} \, d\lambda$$

$$= \frac{\sin\theta_0}{\cos\alpha_0} Q_\xi \, d\xi + \sin\theta_0 \left(\frac{1}{\cos\alpha_0} Q_\lambda + H_\lambda \right) d\lambda \, . \tag{23}$$

13. We can now find the components, in the $\mathbf{i}_1$ and $\mathbf{i}_2$ directions, of the unit-vector increments ε, ε' defined by Eq. (20):

$$\varepsilon_1 = \frac{1}{\sin\theta_0} G_\xi \, d\xi \, , \qquad \varepsilon_2 = \frac{\sin\theta_0}{\cos\alpha_0} Q_\xi \, d\xi \, ; \tag{24}$$

$$\varepsilon_1' = 0 \, , \qquad \varepsilon_2' = \sin\theta_0 \left(\frac{1}{\cos\alpha_0} Q_\lambda + H_\lambda \right) d\lambda \, . \tag{25}$$

14. The next step is to find the cross-sectional area of the ray tube, $A(s)$, at an arbitrary distance s from point B, measured along the reference ray.

Figure 11 shows the cross-section $C_0 C_1 C_2 C_3$ in (x_1, x_2) coordinates, at $s = 0$. The dimensions (f, g, h) of the parallelogram are given by:

$$f = (\mathbf{i}_x \cdot \mathbf{i}_1) \, dx_B(d\xi, 0) = a \sin\theta_0 \, . \, X_\xi \, d\xi \, , \tag{26}$$

$$g = (\mathbf{i}_x \cdot \mathbf{i}_1) \, dx_B(0, d\lambda) = a \sin\theta_0 \, . \, X_\lambda \, d\lambda \, , \tag{27}$$

$$h = (\mathbf{i}_\phi \cdot \mathbf{i}_2) \, a \, d\phi_B(0, d\lambda) = a \cos\alpha_0 \, . \, H_\lambda \, d\lambda \, , \tag{28}$$

where we have used Eqs. (5), (6), (11) and (13).

15. Further along the reference ray, the coordinates of C_0, C_1, C_2, C_3 change as follows:

Point	(x_1, x_2) at $s = 0$	(x_1, x_2) at arbitrary s	
C_0	0, 0	0, 0	
C_1	f, 0	$f + \varepsilon_1 s$,	$\varepsilon_2 s$
C_2	g, h	$g + \varepsilon_1' s$,	$h + \varepsilon_2' s$
C_3	$f + g$, h	$f + g + \varepsilon_1 s + \varepsilon_1' s$,	$h + \varepsilon_2 s + \varepsilon_2' s$

The area of a triangle whose vertices are located at $[(0,0), (a_1,a_2), (b_1,b_2)]$ is $\frac{1}{2} | a_1 b_2 - b_1 a_2 |$. It follows that the ray-tube area at arbitrary s is

$$A(s) = | fh + s(\varepsilon_1 h - \varepsilon_2 g + \varepsilon_2' f) + s^2(\varepsilon_1 \varepsilon_2' - \varepsilon_2 \varepsilon_1') | \, . \tag{29}$$

Appendix B

Note that the leading term gives the cross-sectional area at B (on the edge of the jet); while the s^2 term gives the far-field area, and accounts for spherical spreading.

16. The ray-tube area expression (29) may be written as

$$A(s) = |A_0 + A_1 s + A_2 s^2| \; . \; |d\xi \, d\lambda| \; . \tag{30}$$

The coefficients follow from Eqs. (24) to (28). Thus

$$A_0 = a^2 \sin\theta_0 \cos\alpha_0 \, X_\xi \, H_\lambda \; ; \tag{31}$$

$$A_1 = \left\{ \frac{1}{\sin\theta_0} a \cos\alpha_0 \, G_\xi \, H_\lambda - a \frac{\sin^2\theta_0}{\cos\alpha_0} Q_\xi \, X_\lambda + a \sin^2\theta_0 \left(\frac{1}{\cos\alpha_0} Q_\lambda + H_\lambda \right) X_\xi \right\} ; \tag{32}$$

$$A_2 = \left(\frac{1}{\cos\alpha_0} Q_\lambda + H_\lambda \right) G_\xi \, . \tag{33}$$

17. The explicit functions G, H, Q, X and their derivatives are listed below. From Eqs. (3, 4, 13) of Chapter III,

$$G(\xi, M, C) = \frac{\xi}{C(1 + M\xi)} \, , \quad \left(C = \frac{c_1}{c_0} \; ; \; M = \frac{u}{c_1} \right) ; \tag{34}$$

$$G_\xi = \frac{1}{C(1 + M\xi)^2} \qquad = \frac{C}{\xi^2} G^2 \; ; \tag{35}$$

$$H(\lambda, \frac{r_s}{a}) = \lambda - \sin^{-1}(\sigma_s \sin\lambda) \, , \quad (\sigma_s = r_s/a) \; ; \tag{36}$$

$$H_\lambda = 1 - \frac{\sigma_s \cos\lambda}{\sqrt{1 - \sigma_s^2 \sin^2\lambda}} \qquad = 1 - \beta_1 \, . \tag{37}$$

From Eqs. (4, 6, 7, 8, 12) of Chapter III,

$$Q(\xi, \lambda, M, C, \sigma_s) = \sin\alpha_0 = \left[\frac{1 - \xi^2}{C^2(1 + M\xi)^2 - \xi^2} \right]^{1/2} \sigma_s \sin\lambda \; ; \tag{38}$$

$$Q_\xi = \frac{\xi - C^2(\xi + M)(1 + M\xi)}{(1 - \xi^2)^{1/2} [C^2(1 + M\xi)^2 - \xi^2]^{3/2}} \sigma_s \sin\lambda \; ; \tag{39}$$

$$Q_\lambda = \left[\frac{1 - \xi^2}{C^2(1 + M\xi)^2 - \xi^2} \right]^{1/2} \sigma_s \cos\lambda = Q \cot\lambda \; . \tag{40}$$

Finally, from Eqs. (20), (13) and (18) of Chapter III,

$$X = \frac{d_1}{a} \frac{\xi + M}{\sqrt{1 - \xi^2}} \; ;$$

$$X(\xi, \lambda, M, \sigma_s) = \frac{1}{\sin\lambda} \sin[\lambda - \sin^{-1}(\sigma_s \sin\lambda)] \; . \frac{\xi + M}{\sqrt{1 - \xi^2}}$$

$$= [(1 - \sigma_s^2 \sin^2\lambda)^{1/2} - \sigma_s \cos\lambda] \; . \frac{\xi + M}{\sqrt{1 - \xi^2}} \; ; \tag{41}$$

$$X_\xi = [(1 - \sigma_s^2 \sin^2 \lambda)^{1/2} - \sigma_s \cos \lambda] \frac{1 + M\xi}{(1 - \xi^2)^{3/2}}; \tag{42}$$

$$X_\lambda = \left[\sigma_s \sin \lambda - \frac{\sigma_s^2 \sin \lambda \cos \lambda}{(1 - \sigma_s^2 \sin^2 \lambda)^{1/2}} \right] \cdot \frac{\xi + M}{\sqrt{1 - \xi^2}} . \tag{43}$$

18. The ratio $dA_n/d\Omega_1$ which appears in Eq. (33) of Chapter III can now be calculated as

$$\frac{dA_n}{d\Omega_1} = \frac{A(s)}{|d\xi\, d\lambda|} = |A_0 + A_1 s + A_2 s^2| \ , \tag{44}$$

from Eq. (30) above and Eq. (24) of Chapter III. The coefficients A_0, A_1, A_2 are known from Sections 16 and 17 above. The ray path length s (equal to BM) is given by

$$\frac{s}{a} = \frac{1}{\sin \theta_0} \left[\sqrt{\sigma_m^2 - \sin^2 \alpha_0} - \cos \alpha_0 \right], \qquad (\sigma_m = r_m/a) \tag{45}$$

which follows from Eq. (29) of Chapter III and the relation $s = d_0/\sin \theta_0$.

19. The following special cases of Eq. (45) provide a useful check on the ray-tube area result, Eq. (44).

(1) *Far field* ($\sigma_m \to \infty$):

$$\frac{s}{a} \approx \frac{\sigma_m}{\sin \theta_0} . \tag{46}$$

(2) *Measurement on nozzle lip line* ($\sigma_m = 1$):

$$s/a = 0 . \tag{47}$$

(3) *Source on jet axis* ($\alpha_0 = 0$):

$$\frac{s}{a} = \frac{1}{\sin \theta_0} (\sigma_m - 1) . \tag{48}$$

We consider these special cases in turn, and evaluate Eq. (44) for each one.

20. First, consider special case (1). In the far field, Eqs. (44) and (46) give

$$\frac{dA_n}{d\Omega_1} \approx |A_2| \frac{\sigma_m^2}{\sin^2 \theta_0} a^2 . \tag{49}$$

With A_2 given by Eqs. (33, 35, 37, 40), we get

$$\frac{dA_n}{d\Omega_1} \approx \frac{r_m^2}{\sin^2 \theta_0} \left| \frac{1}{\cos \alpha_0} \sin \alpha_0 \cot \lambda + 1 - \beta_1 \right| \frac{C}{\cos^2 \theta_1} \cos^2 \theta_0$$

$$= r_m^2 \, C \frac{\cos^2 \theta_0}{\sin^2 \theta_0} \frac{1}{\cos^2 \theta_1} |1 - \beta_1 + \beta_0| . \tag{50}$$

The quantities

$$\beta_1 = \frac{\partial \alpha_1}{\partial \lambda} = 1 - H_\lambda , \tag{51}$$

$$\beta_0 = \frac{\partial \alpha_0}{\partial \lambda} = \frac{1}{\cos \alpha_0} Q_\lambda = \tan \alpha_0 \cot \lambda \tag{52}$$

were introduced in Appendix A. Equation (50) yields

$$dA_m = \frac{1}{\sin\theta_0} dA_n \qquad \text{(see Fig. 5)}$$

$$= r_m^2 \, C \frac{\cos^2\theta_0}{\sin^3\theta_0} \frac{|d\xi \, d\lambda|}{\cos^2\theta_1} \cdot |1 - \beta_1 + \beta_0|$$

$$= r_m^2 \, C \frac{\cos^2\theta_0}{\sin^3\theta_0} \frac{\sin\theta_1}{\cos^2\theta_1} \cdot |1 - \beta_1 + \beta_0| \cdot |d\lambda \, d\theta_1| \,, \tag{53}$$

which agrees with Eq. (9) of Appendix A.

21. Next, consider special case (2). When $r_m = a$, we have $s = 0$ and Eq. (44) gives

$$\frac{dA_n}{d\Omega_1} = |A_0|$$

$$= a^2 \, |\sin\theta_0 \cos\alpha_0 \, X_\xi H_\lambda|$$

$$= a^2 \, |\sin\theta_0 \cos\alpha_0 \frac{\sin\phi_B}{\sin\lambda} \cdot \frac{\cos\theta_1}{C\cos\theta_0} \cdot \frac{1}{\sin^3\theta_1} H_\lambda| \,; \tag{54}$$

here we have used Eq. (42) and converted the result back into the notation of Chapter III, using angles ϕ_B and θ_0. Since

$$d\Omega_1 = |d\xi \, d\lambda| = \sin\theta_1 \, |d\theta_1 \, d\lambda| \,, \tag{55}$$

Eq. (54) gives

$$dA_n(r_m{=}a) = a^2 H_\lambda \cdot \cos\alpha_0 \frac{\sin\phi_B}{\sin\lambda} \cdot \frac{\sin\theta_0}{C\cos\theta_0} \frac{\cos\theta_1}{\sin^2\theta_1} \cdot |d\theta_1 \, d\lambda| \,. \tag{56}$$

Equation (56) agrees with Chapter III, Eq. (49), where H_λ is written as $F(\lambda)$. This provides a second check on our general result, Eq. (44) above. The A_0 and A_2 terms have now both been verified, but we still need a check on A_1; a partial check is provided in the next two sections, where we consider on-axis sources.

22. Our final check on Eq. (44) is provided by special case (3). When $r_s = 0$ (i.e. $\bar{\sigma_s} = 0$), α_0 becomes zero and the coefficients A_0, A_1, A_2 simplify as follows.

$$H = \phi_B \to \lambda \,; \qquad H_\xi = 0 \,, \; H_\lambda = 1 \,. \tag{57}$$

$$Q = \sin\alpha_0 \to 0 \,; \qquad Q_\xi = 0 \,, \; Q_\lambda = 0 \,. \tag{58}$$

$$X \to \frac{\xi + M}{\sqrt{1 - \xi^2}} \quad (\text{since } d_1 \to a);$$

$$X_\xi = \frac{1 + M\xi}{(1 - \xi^2)^{3/2}} = \frac{\cos\theta_1}{C\cos\theta_0} \cdot \frac{1}{\sin^3\theta_1} \,, \qquad X_\lambda = 0 \,. \tag{59}$$

Thus

$$A_0 = a^2 \sin\theta_0 \cdot \frac{1}{C\cos\theta_0} \frac{\cos\theta_1}{\sin^3\theta_1} \,; \tag{60}$$

$$A_1 = a \, C \frac{\cos^2\theta_0}{\cos^2\theta_1} \frac{1}{\sin\theta_0} + a \sin^2\theta_0 \cdot \frac{1}{C\cos\theta_0} \frac{\cos\theta_1}{\sin^3\theta_1} \,; \tag{61}$$

$$A_2 = C\frac{\cos^2\theta_0}{\cos^2\theta_1}. \tag{62}$$

23. The ray path length s in this case is given by Eq. (48):

$$s = \frac{1}{\sin\,\theta_0}(r_m - a)\ . \tag{62}$$

Substituting Eqs. (60–62) in Eq. (44) gives, for on-axis sources,

$$\begin{aligned}\frac{1}{a^2}\frac{dA_n}{d\Omega_1} = \Bigg| & \frac{1}{C}\tan\,\theta_0\frac{\cos\,\theta_1}{\sin^3\theta_1} \\ & + \left(\frac{r_m}{a} - 1\right)\left(C\cot^2\theta_0\frac{1}{\cos^2\theta_1} + \frac{1}{C}\tan\,\theta_0\frac{\cos\,\theta_1}{\sin^3\,\theta_1}\right) \\ & + \left(\frac{r_m}{a} - 1\right)^2 C\cot^2\theta_0\frac{1}{\cos^2\theta_1}\Bigg|\ .\end{aligned} \tag{63}$$

The constant terms (i.e. those independent of r_m) on the right-hand side cancel, leaving

$$\begin{aligned}\frac{1}{a^2}\frac{dA_n}{d\Omega_1} &= \left|\left(\frac{r_m}{a}\right)^2 C\cot^2\theta_0\frac{1}{\cos^2\theta_1} + \left(\frac{r_m}{a}\right)\left(\frac{1}{C}\tan\,\theta_0\frac{\cos\,\theta_1}{\sin^3\theta_1} - C\cot^2\theta_0\frac{1}{\cos^2\theta_1}\right)\right| \\ &= C\cot^2\theta_0\frac{1}{\cos^2\theta_1}\left|\left(\frac{r_m}{a}\right)^2 + \left(\frac{r_m}{a}\right)\left\{\frac{1}{C^2}\left(\frac{\tan\,\theta_0}{\tan\,\theta_1}\right)^3 - 1\right\}\right|\ ,\end{aligned} \tag{64}$$

which agrees with the result in Chapter III, Eq. (53).

24. All three special cases listed in Section 19 above have now been checked; in each case our general result, Eq. (44), reduces to the previously known result from Chapter III. The only terms not checked in this process are the Q_ξ and Q_λ terms in Eq. (32). It therefore appears safe to base a numerical study on Equation (44), with the three coefficients (A_0, A_1, A_2) given by Eqs. (31–43).

List of Figures

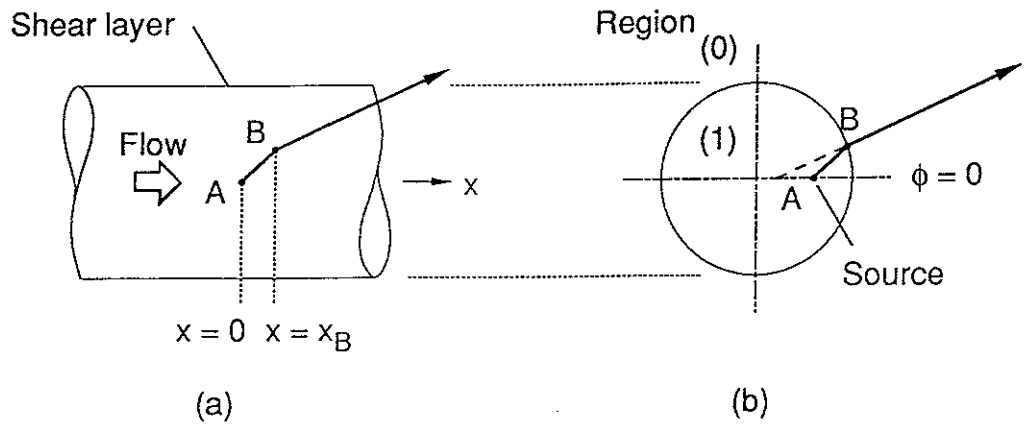

Figure 1 Ray geometry. (a) Side view. (b) View along x axis.

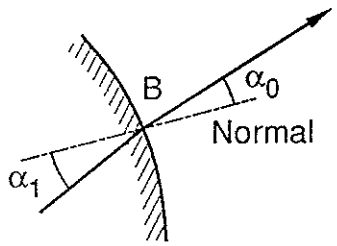

Figure 2 Refraction in transverse plane.

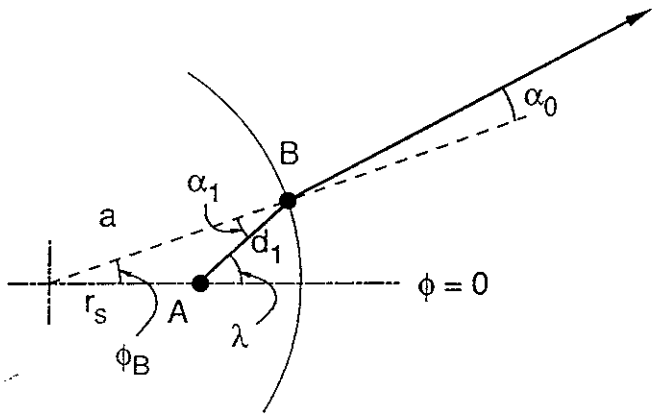

Figure 3 Source emission angle and ray refraction in the transverse plane. Transverse distance AB = d_1.

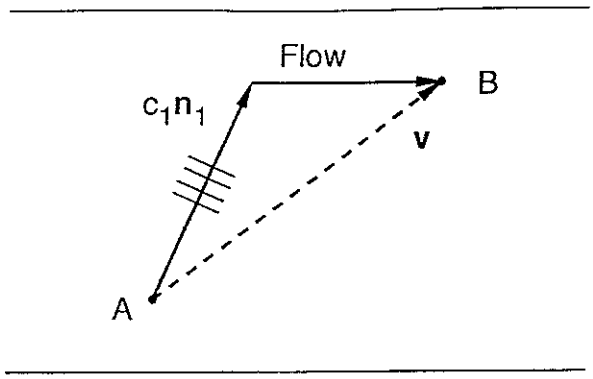

Figure 4 Ray diagram for sound propagation from source (at A) to jet boundary (at B). Ray velocity **v** is resultant of c_1 in the wavenormal direction, and U in the axial direction.

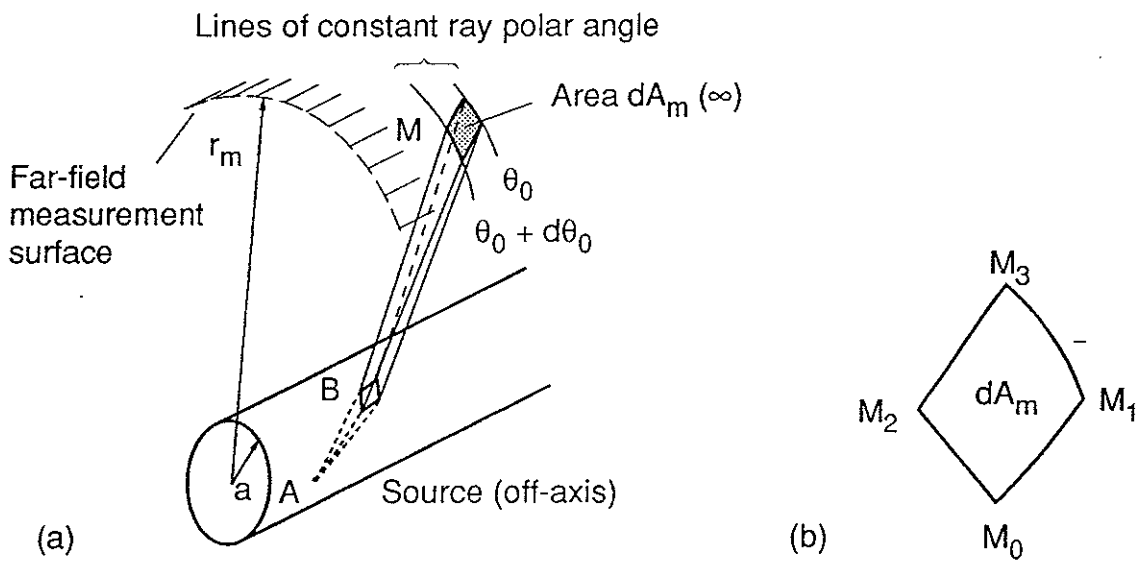

Figure 5 (a) Ray tube geometry between source and far-field point.

(b) Enlargement of ray tube intersection with the cylindrical surface $r = r_m$, in the farfield ($r_m >> a$).

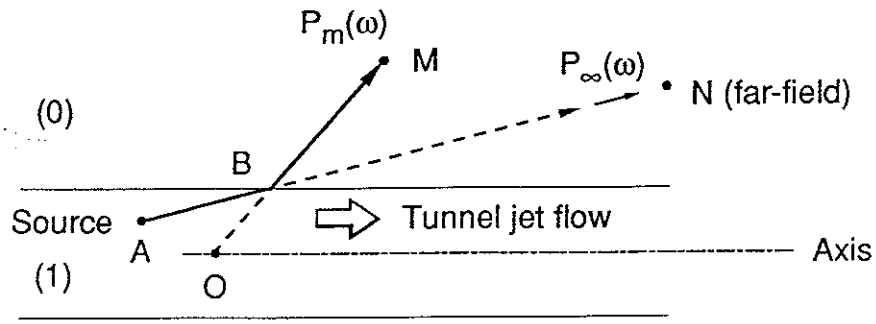

Figure 6 Flight simulation versus the true flight situation: comparison of ray paths.

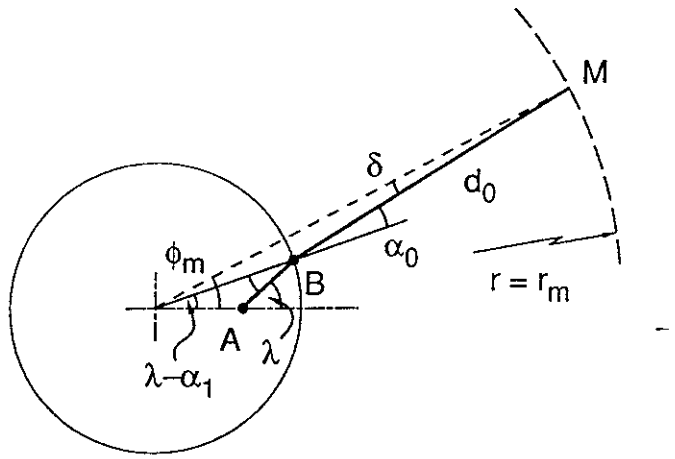

Figure 7 Geometry for calculation of measurement azimuth angle. Transverse distance BM = d_0.

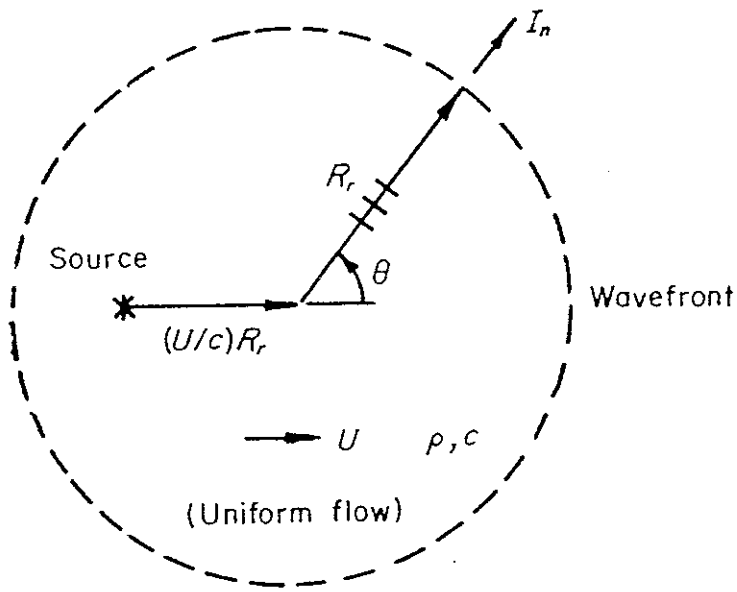

Figure 8 Definition of intensity component normal to wavefront.

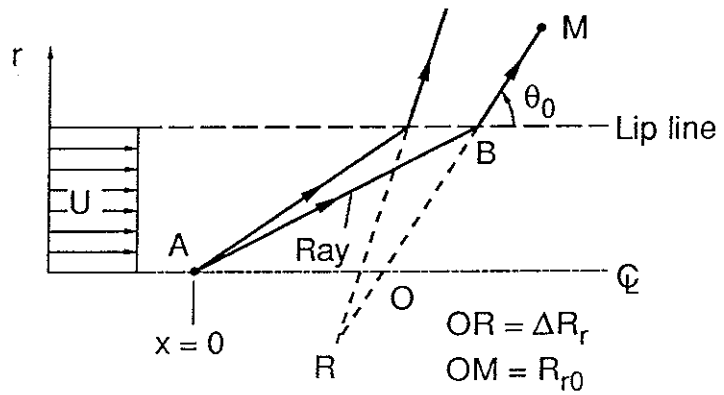

Figure 9 Near-field correction for a source on the jet axis.

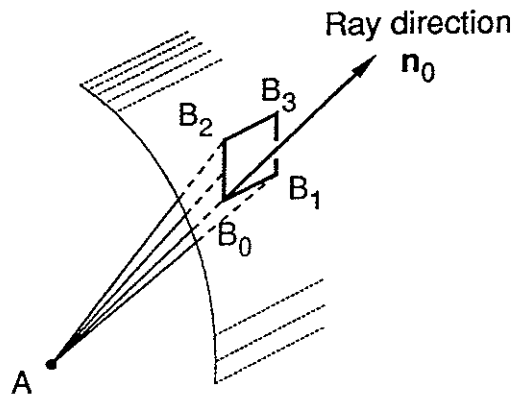

Figure 10 Intersection of ray tube with the edge of the jet (r = a). Also shown is the emerging reference ray with direction $\mathbf{n}_0$.

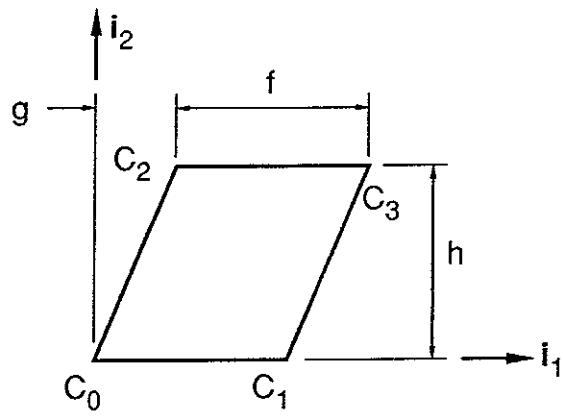

Figure 11 Cross-section of ray tube at point B, viewed looking back along the reference ray towards B_0; the unit vector $\mathbf{n}_0$ points out of the page. The three unit vectors $\mathbf{i}_1$, $\mathbf{i}_2$, $\mathbf{n}_0$ form a right-handed orthogonal set, and remain constant along the ray.

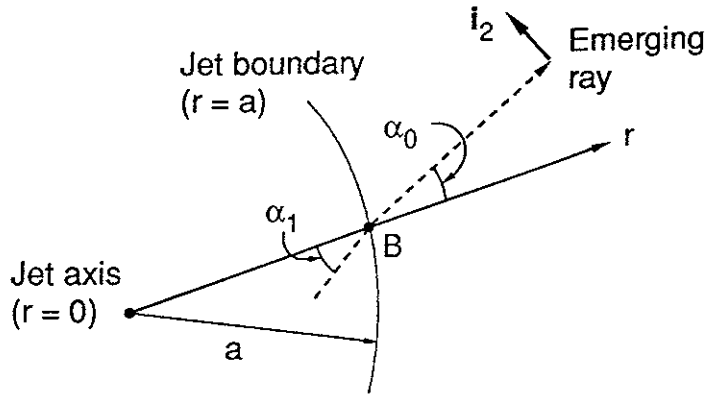

Figure 12 View in $\mathbf{i}_x$ direction (parallel to jet axis), showing the incident and transmitted ray angles at B and the unit vector $\mathbf{i}_2$ normal to the emerging ray in the transverse plane.

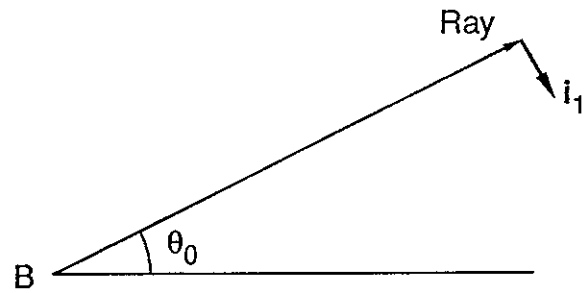

Figure 13 View in $\mathbf{i}_2$ direction, showing the emerging ray (as in Figure 12) and the unit vector $\mathbf{i}_1$ perpendicular to the ray.